Data-driven discovery of electron continuity equations in electron swarm map for determining electron transport coefficients in argon

Data-driven discovery of electron continuity equations in electron swarm map for determining electron transport coefficients in argon

S Kawaguchi [1*], K Takahashi [1], and K Satoh[1]

[1] *Division of Information and Electronic Engineering, Graduate School of Engineering, Muroran Institute of Technology, Muroran, Hokkaido, 050-8585, Japan*

E-mail: skawaguchi@mmm.muroran-it.ac.jp

Abstract. In this study, we develop a novel method for determining electron transport coefficients from electron swarm maps measured by a scanning drift-tube experiment. In our method, two types of electron continuity equations that describe either the spatial or the temporal evolution of an electron swarm are discovered in the electron swarm map. The electron transport coefficients can be determined from the coefficients in the discovered equations. Therefore, we can determine the Townsend ionization coefficient, ionization rate coefficient, center-of-mass drift velocity, mean arrival-time drift velocity, longitudinal diffusion coefficient, and longitudinal third-order transport coefficient. These transport coefficients in argon are determined over a wide range of reduced electric fields, *E/N*, from 29.7 to 1351.6 Td (1 Td = 10^{-21} Vm^2) using our method. We establish that the consideration of high-order transport coefficients, which have been systematically ignored so far, is important for the proper determination of low-order transport coefficients, specifically the electron drift velocity and longitudinal diffusion coefficient, in the presence of ionization growth.

1. Introduction

Electron swarm experiments play an important role in providing electron transport coefficients, which are essential for the development of the transport theory of electron swarms in weakly ionized plasmas as well as for plasma simulation [1]. Electron transport coefficients are also vital for constructing a self-consistent set of electron collision cross sections [2-4], which are required for calculating electron velocity distribution and electron energy distribution functions by Boltzmann equation analysis and Monte Carlo simulation (MCS) [5-7].

The scanning drift tube experiment recently developed by Donkó and co-workers [8-11] is the electron swarm experiment which allows the measurement of the spatiotemporal evolution of an isolated electron swarm in a drift tube under homogeneous DC electric fields with high spatial and temporal resolutions. The measured evolution of the electron swarm is referred to as the electron swarm map.

Donkó and co-workers approximated the measured electron swarm map to determine the electron transport coefficients as

$$n(t,z) = \frac{n_0}{(4\pi D_L)^{1/2}} \exp\left[R_i t - \frac{(z - W_r t)^2}{4\pi D_L}\right], \tag{1}$$

where n_0 is the electron number density at $t = 0$ and $z = 0$, R_i is the ionization collision frequency, W_r is the center-of-mass drift velocity (also referred to as the bulk drift velocity), and D_L is the longitudinal diffusion coefficient. Equation (1) is an analytical solution of the drift-diffusion equation

$$\frac{\partial n}{\partial t} = R_i n - W_r \frac{\partial n}{\partial z} + D_L \frac{\partial^2 n}{\partial z^2}. \tag{2}$$

In certain types of electron swarm experiments the drift-diffusion equation is the basis for determining electron transport coefficients. However, the evolution of electron swarms is rigorously described by the electron continuity equation, which includes terms regarding high-order gradients of $n(t, z)$ and their corresponding high-order transport coefficients [12, 13], which have been systematically ignored so far.

The effect of considering high-order gradients and the corresponding high-order transport coefficients on determining the low-order transport coefficient, such as R_i, W_r, and D_L, is unclear. Kawaguchi *et al.* [14] established that the value of D_L in nitrogen determined based on equation (1) differs from that determined from the time variation of the spatial moment of the electron distribution in high reduced electric fields. This indicates that the analysis of the electron swarm map based on equation (1) would yield inaccurate electron transport coefficients in the presence of ionization growth.

Recently, data-driven discovery of partial differential equations (PDEs), in which physical laws and governing equations in data have been discovered, has emerged [15, 16]. Physic-informed neural networks (PINNs) are data-driven methods for solving and discovering PDEs using deep learning [17, 18]. The basic idea of PINNs for discovering PDEs is that an artificial neural network (ANN), which has a high capability for representing non-linear functions, is trained to approximate the function adapted to PDEs and the given data. The PDE coefficients are treated as tunable parameters and optimized together with the training of the ANN.

In this study, we develop a novel approach for determining the electron transport coefficients in an electron swarm map. The electron continuity equation is discovered in the electron swarm map by leveraging PINNs. The electron transport coefficients are obtained from the coefficients in the discovered continuity equation. Our method allows us to deal with the electron continuity equation directly, making it unnecessary to assume an analytical form for the electron swarm map.

The collaboration between the PINNs and electron swarm experiments enables us to measure the low-order and high-order transport coefficients more accurately. Using our method, we determine many types of electron transport coefficients in argon, including the Townsend ionization coefficient, ionization rate coefficient, center-of-mass drift velocity, mean arrival-time drift velocity, longitudinal diffusion coefficient, and longitudinal third-order transport coefficient.

2. Electron continuity equations and corresponding electron transport coefficients

We clarify two types of electron continuity equations, which describe either the temporal or spatial evolution of an isolated electron swarm under DC uniform electric fields, $\boldsymbol{E}$ = (0, 0, -E). The corresponding electron transport coefficients are defined. The hydrodynamic equilibrium regime is considered here; therefore, the transport coefficient is independent of time and position.

The temporal evolution of the electron swarm is written as [12, 19]

$$\frac{\partial n(t,z)}{\partial t} = \omega_0 n(t,z) - \omega_1 \frac{\partial n(t,z)}{\partial z} + \omega_2 \frac{\partial^2 n(t,z)}{\partial z^2} - \omega_3 \frac{\partial^3 n(t,z)}{\partial z^3} + \cdots. \quad (3)$$

The transport coefficients corresponding to equation (3) are called ω parameters. The first four ω parameters are defined as follows:

$$\omega_0 = R_i = \frac{d}{dt} \ln N_e\,(t), \quad (4)$$

$$\omega_1 = W_r = \frac{d}{dt} \langle z \rangle (t), \quad (5)$$

$$\omega_2 = D_L = \frac{1}{2!} \frac{d}{dt} \langle Z^2 \rangle (t), \quad (6)$$

$$\omega_3 = Q_\mathrm{L} = \frac{1}{3!} \frac{d}{dt} \langle Z^3 \rangle (t), \quad (7)$$

where

$$N_e(t) = \int_{-\infty}^{\infty} n(t,z) dz\,, \quad (8)$$

$$\langle z \rangle (t) = N_e^{-1}(t) \int_{-\infty}^{\infty} z n(t,z) dz\,, \quad (9)$$

$$Z = z - \langle z \rangle. \quad (10)$$

ω_0, ω_1, and ω_2 are identical to R_i, W_r, and D_L, respectively. ω_3 is the longitudinal third-order transport coefficient, Q_L.

The spatial evolution of the electron swarm can be describes as [19]

$$\frac{\partial n(t,z)}{\partial z} = \alpha_0 n(t,z) - \alpha_1 \frac{\partial n(t,z)}{\partial t} + \alpha_2 \frac{\partial^2 n(t,z)}{\partial t^2} - \alpha_3 \frac{\partial^3 n(t,z)}{\partial t^3} + \cdots. \quad (11)$$

The transport coefficients corresponding to equation (11) are called α parameters. Equation (11) is equivalent and complementary to equation (3). The first four α parameters are defined as follows:

$$\alpha_0 = \alpha_\mathrm{T} = \frac{d}{dz} \ln N_e\,(z), \quad (12)$$

$$\alpha_1 = W_m^{-1} = \frac{d}{dz}\langle t\rangle(z), \tag{13}$$

$$\alpha_2 = \frac{1}{2!}\frac{d}{dz}\langle T^2\rangle(z), \tag{14}$$

$$\alpha_3 = \frac{1}{3!}\frac{d}{dz}\langle T^3\rangle(z), \tag{15}$$

where

$$N_e(z) = \int_0^\infty n(t,z)dt\,, \tag{16}$$

$$\langle t\rangle(z) = N_e^{-1}(z)\int_0^\infty tn(t,z)dt\,, \tag{17}$$

$$T = t - \langle t\rangle. \tag{18}$$

α_0 and α_1 are identical to the Townsend first ionization coefficient, α_{T}, and the reciprocal of the mean arrival-time drift velocity, W_{m}, respectively.

3. Methodology

Figure 1 shows a schematic of the data-driven discovery of the electron continuity equations in the electron swarm map. An ANN is used to represent the electron swarm map. The architecture of the ANN used in this study is described in section 3.1. The procedure for training the ANN and discovering the electron continuity equations is described in section 3.2. The preparation of the training dataset, which contains examples of an electron swarm map, is described in section 3.3.

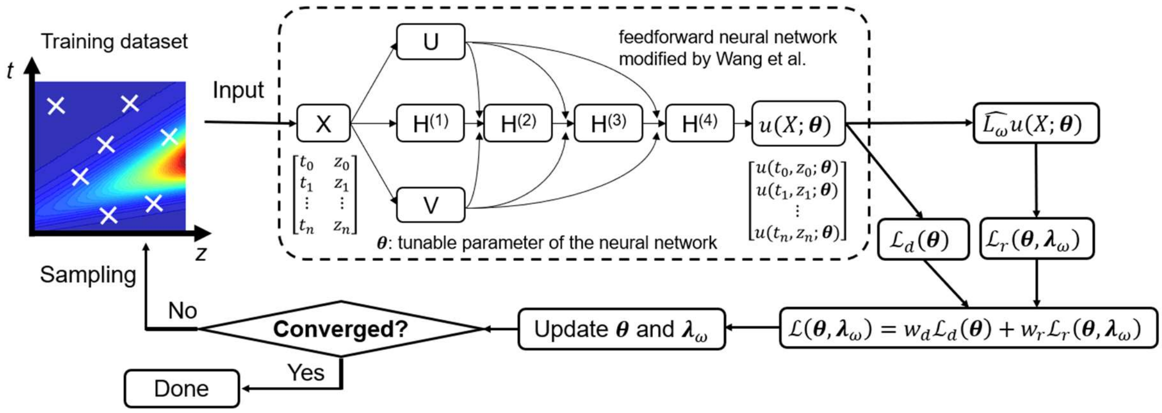

Figure 1. Schematic diagram of data-driven discovery of electron continuity equations.

3.1 ANN

We employed a multilayer feedforward neural network modified by Wang *et al*. [20] to represent the electron swarm map. The input of the neural network is the coordinates of points, *t* and *z*, which are stored in a matrix *X*. The output of the neural network $u(X;\boldsymbol{\theta})$ is calculated as follows:

$$U = \sigma(XW_1 + b_1), \tag{19}$$

$$V = \sigma(XW_2 + b_2), \tag{20}$$

$$H^{(1)} = \sigma\left(XW_{z,1} + b_{z,1}\right), \tag{21}$$

$$Z^{(k)} = \sigma\left(H^{(k)}W_{z,k} + b_{z,k}\right) \quad (k = 1,2,\dots,L), \tag{22}$$

$$H^{(k+1)} = \left(1 - Z^{(k)}\right) \odot U + Z^{(k)} \odot V \ (k = 1,2,\dots,L), \tag{23}$$

$$u(X;\boldsymbol{\theta}) = H^{(L+1)}W + b. \tag{24}$$

Here, L denotes the number of hidden layers, σ denotes a non-linear activation function, and $\odot$ denotes the Hadamard product (element-wise multiplication). W_1, W_2, $W_{z,k}$, and W are the weight matrices. b_1, b_2, $b_{z,k}$, and b are the bias matrices. The elements of these matrices are tunable parameters of the ANN, which are denoted as $\boldsymbol{\theta}$.

3.2 Training the ANN and discovering the electron continuity equations

First, we discover the following non-linear PDE in the training dataset:

$$\left[\frac{\partial}{\partial t} - \lambda_{\omega 0} + \lambda_{\omega 1}\frac{\partial}{\partial z} - \lambda_{\omega 2}\frac{\partial^2}{\partial z^2} + \lambda_{\omega 3}\frac{\partial^3}{\partial z^3}\right]u(t,z) = 0. \tag{25}$$

The PDE coefficients, $\boldsymbol{\lambda}_\omega = (\lambda_{\omega 0}, \lambda_{\omega 1}, \lambda_{\omega 2}, \lambda_{\omega 3})$, are treated as tunable parameters. Hereafter, equation (25) is written as $\hat{L}_\omega u(t,x) = 0$ with the operator $\hat{L}_\omega$. The latent solution of equation (25), $u(t,z)$, is represented by the ANN, $u(t,z;\boldsymbol{\theta})$.

All tunable parameters, $\boldsymbol{\lambda}_\omega$ and $\boldsymbol{\theta}$, are optimized to minimize the following loss function:

$$\mathcal{L}(\boldsymbol{\theta}, \boldsymbol{\lambda}_\omega) = w_r \mathcal{L}_r(\boldsymbol{\theta}, \boldsymbol{\lambda}_\omega) + w_d \mathcal{L}_d(\boldsymbol{\theta}), \tag{26}$$

where

$$\mathcal{L}_r(\boldsymbol{\theta}, \boldsymbol{\lambda}_\omega) = \frac{1}{N_r}\sum_{i=1}^{N_r}\left|\hat{L}_\omega u\left(t_i^{(r)}, z_i^{(r)}; \boldsymbol{\theta}\right)\right|, \tag{27}$$

and

$$\mathcal{L}_d(\boldsymbol{\theta}) = \frac{1}{N_\mathrm{d}}\sum_{i=1}^{N_d}\left|u\left(t_i^{(d)}, z_i^{(d)}; \boldsymbol{\theta}\right) - n_i^{(d)}\right|. \tag{28}$$

Here, $n_i^{(d)}$ denotes the value of the electron swarm map at $\left(t_i^{(d)}, z_i^{(d)}\right)$. The values of $\mathcal{L}_r$ and $\mathcal{L}_d$ indicate how well the function represented by the ANN satisfies equation (25) and the training dataset, respectively. Owing to the representation $u(t,z;\boldsymbol{\theta})$ by the ANN, the value of $\hat{L}_\omega u$ can be calculated analytically using automatic differentiation. The balance between $\mathcal{L}_r$ and $\mathcal{L}_d$ is controlled by w_r and w_d. In this study, $w_r = 1$, $w_d = 100$.

When $\mathcal{L}$ converges, the ANN represents the electron swarm map adapted to the training dataset and equation (25) with optimized $\boldsymbol{\lambda}_\omega$. Simultaneously, by comparing equations (3) and (25), the optimized $\boldsymbol{\lambda}_\omega$ represents $\omega_0 - \omega_3$ given that high-order gradients and corresponding transport coefficients can be ignored.

Another form of the electron continuity equation

$$\left[\frac{\partial}{\partial z} - \lambda_{\alpha 0} + \lambda_{\alpha 1}\frac{\partial}{\partial t} - \lambda_{\alpha 2}\frac{\partial^2}{\partial t^2} + \lambda_{\alpha 3}\frac{\partial^3}{\partial t^3}\right] u(t,z) = 0, \tag{29}$$

is also discovered. $\boldsymbol{\lambda}_\alpha = (\lambda_{\alpha 0}, \lambda_{\alpha 1}, \lambda_{\alpha 2}, \lambda_{\alpha 3})$ is a tunable parameter, and equation (29) is written as $\hat{L}_\alpha u(t,z) = 0$ with the operator $\hat{L}_\alpha$. The procedure for optimizing $\boldsymbol{\theta}$ and $\boldsymbol{\lambda}_\alpha$ is the same, except for replacing $\mathcal{L}_r(\boldsymbol{\theta}, \boldsymbol{\lambda}_\omega)$ in the loss function as follows:

$$\mathcal{L}_r(\boldsymbol{\theta}, \boldsymbol{\lambda}_\alpha) = \frac{1}{N_r}\sum_{i=1}^{N_r}\left|\hat{L}_\alpha u\left(t_i^{(r)}, z_i^{(r)}; \boldsymbol{\theta}\right)\right|. \tag{30}$$

Comparing equations (11) and (29), the optimized $\boldsymbol{\lambda}_\alpha$ represents $\alpha_0 - \alpha_3$ given that high-order gradients and corresponding transport coefficients can be ignored.

Points $\left(t_i^{(d)}, z_i^{(d)}\right) \in \Omega$ are randomly sampled at each iteration from the training dataset, where Ω is the input domain ($\Omega = [0,1]^2$). Points $\left(t_i^{(r)}, z_i^{(r)}\right) \in \Omega$ are sampled using the evolutionary sampling method [21]. We initially sample points $\left(t_i^{(r)}, z_i^{(r)}\right)$ from a uniform distribution $\mathcal{U}(\Omega)$. At each iteration, the sampling points satisfying $\left|\hat{L}_\omega u\left(t_i^{(r)}, z_i^{(r)}; \boldsymbol{\theta}\right)\right| > \mathcal{L}_r(\boldsymbol{\theta}, \boldsymbol{\lambda}_\omega)$ or $\left|\hat{L}_\alpha u\left(t_i^{(r)}, z_i^{(r)}; \boldsymbol{\theta}\right)\right| > \mathcal{L}_r(\boldsymbol{\theta}, \boldsymbol{\lambda}_\alpha)$ are retained, and the other sampling points are rejected. To compensate for the rejected points, we resample the points from $\mathcal{U}(\Omega)$. The retained and resampled points are the sampling points used in the next iteration.

The procedure for optimizing the tunable parameters in determining ω parameters is summarized as follows:

(1) Initialize all tunable parameters at the first iteration.

(2) Sample points $\left(t_i^{(r)}, z_i^{(r)}\right)$ ($i = 1, 2, ..., N_r$) from $\mathcal{U}(\Omega)$.

(3) Sample points $\left(t_i^{(d)}, z_i^{(d)}\right)$ ($i = 1, 2, ..., N_d$) from the training dataset.

(4) Calculate $\mathcal{L}(\boldsymbol{\theta}, \boldsymbol{\lambda}_\omega)$.

(5) Update all tunable parameters to minimize the value of $\mathcal{L}(\boldsymbol{\theta}, \boldsymbol{\lambda}_\omega)$.

(6) Resample points $\left(t_i^{(r)}, z_i^{(r)}\right)$ using the evolutionary sampling method.

(7) Repeat steps (3) – (6) until the value of $\mathcal{L}(\boldsymbol{\theta}, \boldsymbol{\lambda}_\omega)$ converges.

3.3 Preparing the training dataset

Figure 2 shows the procedure used to prepare the training dataset. Because we only focus on the hydrodynamic equilibrium regime, we extract the regime from the electron swarm map. We checked the time from $t = 0$ and distance from $z = 0$ required to reach the equilibrium regime using the MCS described below. The values of t, z, and $n(t, z)$ in the extracted swarm map are normalized to be distributed between 0 and 1. The normalized electron swarm map is used as the training dataset.

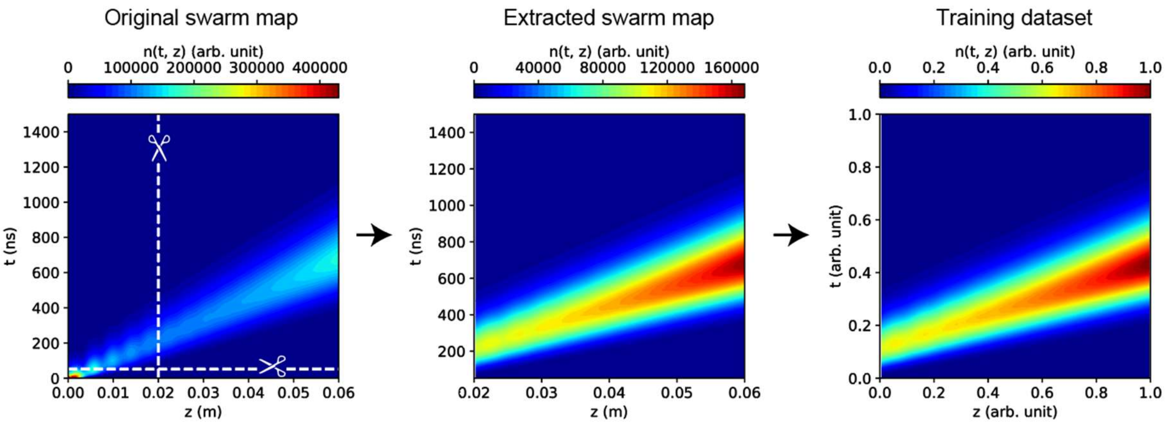

Figure 2. Procedure for preparing the training dataset.

4. Results and discussion

First, we benchmark the ability of our method to discover the electron continuity equation using the MCS results in section 4.1. Thereafter, we determine the electron transport coefficients in argon using the electron swarm map measured by the scanning drift tube [10, 11] in section 4.2.

In this work, we used the ANN, which has four hidden layers with 50 units each. A hyperbolic tangent function is used as an activation function. The weight and bias matrices are initialized using the Glorot initialization method [22]. The components of $\boldsymbol{\lambda}_\omega$ and $\boldsymbol{\lambda}_\alpha$ are initially set to 1. All tunable parameters are optimized using Adam [23]. The initial learning rate is 10^{-2} and decays every 5000 iterations with a decay rate of 0.9. The number of sampling points is set to $N_r = 1000$ and $N_d = 1000$.

4.1 Benchmark study

The electron swarm map is obtained from our MCS, and the obtained electron swarm map is used as the training dataset. Our method is benchmarked by comparing the electron transport coefficients determined from the training dataset with those calculated from the MCS. The details of the MCS were provided in Refs. [3, 7]. The motion of electrons in argon under a DC uniform electric field $\boldsymbol{E} = (0, 0, -E)$ is traced using the Monte Carlo method. The initial electrons are generated at $t = 0$ and $z = 0$, and their electron energy distribution is assumed as a Maxwell–Boltzmann distribution with a mean energy of 1.0 eV. No walls or boundaries are considered in the simulation. The electron velocity and position after τ are updated by

$$\boldsymbol{v}(t+\tau) = \boldsymbol{v}(t) + \frac{q\boldsymbol{E}}{m}\tau \tag{31}$$

$$\boldsymbol{r}(t+\tau) = \boldsymbol{r}(t) + \boldsymbol{v}(t)\tau + \frac{1}{2}\frac{q\boldsymbol{E}}{m}\tau^2 \quad (32)$$

where q denotes the electron charge and m denotes the electron mass. The flight time between successive collisions is calculated using the null collision method [24]. The electron position and velocity are sampled at constant time intervals. The electron swarm map and electron transport coefficients are obtained from sampling data. The gas temperature, T, is set as 293 K. The gas pressure, p, is set to the same value as that in the scanning drift tube experiment [10, 11], ranging from p = 0.08 to 2.1 Torr. The value of the reduced electric field, E/N, in the simulation ranges from 35.9 to 1351.6 Td, where N denotes the number density of gas molecules. The electron collision cross section set of argon reported by Yanguas-Gil *et al.* [25] is used.

Figure 3 shows the electron swarm map at E/N = 438 Td obtained from the MCS and predicted by the trained ANN. The absolute error between the two swarm maps is also presented. The maximum length for recording the electron swarm map is set to 6 cm, which is almost the same as the length in the scanning drift tube experiment. The trained ANN reproduces the electron swarm map obtained from the MCS well. The mean absolute error is 1.63×10^{-3}. We find almost the same result in the other conditions, indicating that the ANN used in this study can represent the electron swarm map in the range of E/N considered here.

When we observe the spatial electron distribution, the spatial variation of the electron swarm map at a fixed time, the distribution could spread beyond z = 6 cm over time. The spatial electron distribution was not necessarily captured from the rising and falling edges in the scanning drift tube experiment because of the maximum length of the drift tube. Conversely, when we observe the temporal electron distribution, the temporal variation of the electron swarm map at a fixed position, the distribution is well captured, making it easy to discover α parameters appropriately rather than ω parameters in the electron swarm map.

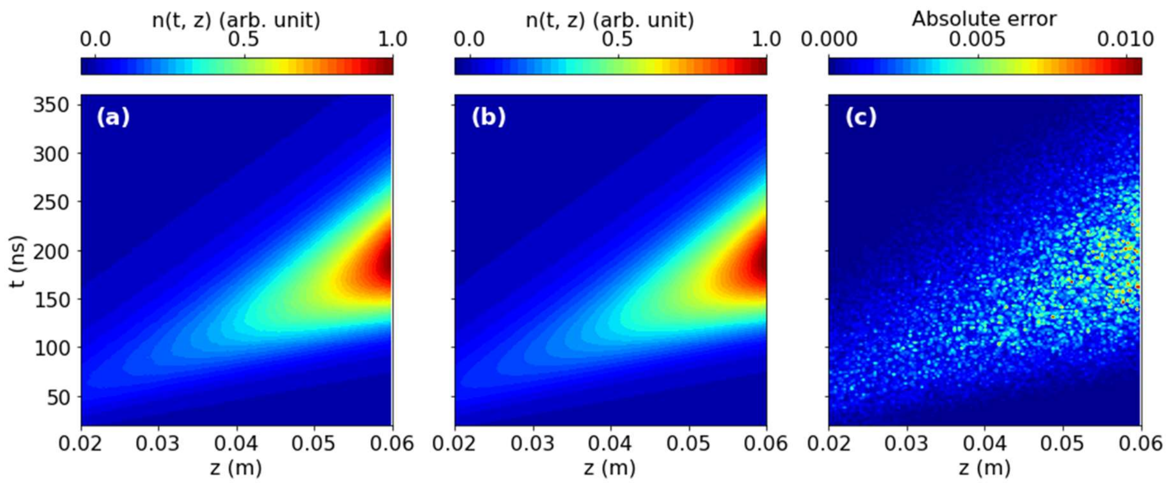

Figure 3. Electron swarm map at E/N = 438 Td. (a) Swarm map obtained from our MCS. (b) Swarm map predicted by the trained ANN. (c) Absolute error between the two swarm maps.

Figure 4 shows the relative difference between the ω parameter calculated from the MCS and that determined from the electron swarm map using the present method as functions of E/N as shown in solid lines. The relative difference is defined by

$$\Delta = \frac{\zeta_{\mathrm{MAP}} - \zeta_{\mathrm{MCS}}}{\zeta_{\mathrm{MCS}}} \times 100\ (\%), \tag{33}$$

where ζ_{MCS} and ζ_{MAP} denote the transport coefficient obtained from the MCS and the electron swarm map, respectively. Here, we also calculated the relative difference for $\omega_0 - \omega_2$ determined by fitting equation (1) to the swarm map and discovering the drift-diffusion equation,

$$\left[\frac{\partial}{\partial t} - \lambda_{\omega 0} + \lambda_{\omega 1}\frac{\partial}{\partial z} - \lambda_{\omega 2}\frac{\partial^2}{\partial z^2}\right] u(t,z) = 0, \tag{34}$$

which is obtained by removing the fifth term on the right-hand side of equation (25). In general, the relative difference tends to increase with E/N values. The large relative difference may be attributed to truncating the electron continuity equation. The values of $\omega_0 - \omega_2$ from fitting equation (1) are found to be the least consistent with those calculated from the MCS. The values of $\omega_0 - \omega_2$ determined from discovering the drift-diffusion equation is not necessarily consistent with those from equation (1). We found that the values of $\omega_0 - \omega_2$ determined from discovering equation (25) are the most consistent with those from the MCS, indicating the need for considering the high-order transport coefficient to describe the spatiotemporal evolution of the electron swarm properly, especially in the high E/N region. The values of ω_0, ω_1, ω_2, and ω_3 determined from equation (25) were up to 5.2%, 7.5%, 35%, and 82% lower than those calculated from the MCS.

Figure 5 shows the relative difference between the α parameter calculated from the MCS and that determined using our method as a function of E/N. Here, we also determined the $\alpha_0 - \alpha_2$ from discovering

$$\left[\frac{\partial}{\partial z} - \lambda_{\alpha 0} + \lambda_{\alpha 1}\frac{\partial}{\partial t} - \lambda_{\alpha 2}\frac{\partial^2}{\partial t^2}\right] u(t,z) = 0, \tag{35}$$

which is obtained by removing the fifth term on the right-hand side of equation (29). Compared to the ω parameter, the relative difference in the α parameter is not significantly affected by E/N values. The discrepancy in the trend of the relative difference for the ω and α parameters is attributed to the difference in the temporal and spatial distributions captured in the electron swarm map. The effect of considering the third-order transport coefficient clearly appears in the relative difference for α_1. The values of α_0, α_1, α_2, and α_3 determined from equation (29) were up to 7.4%, 1.6%, 22%, and 45% lower than those calculated from the MCS.

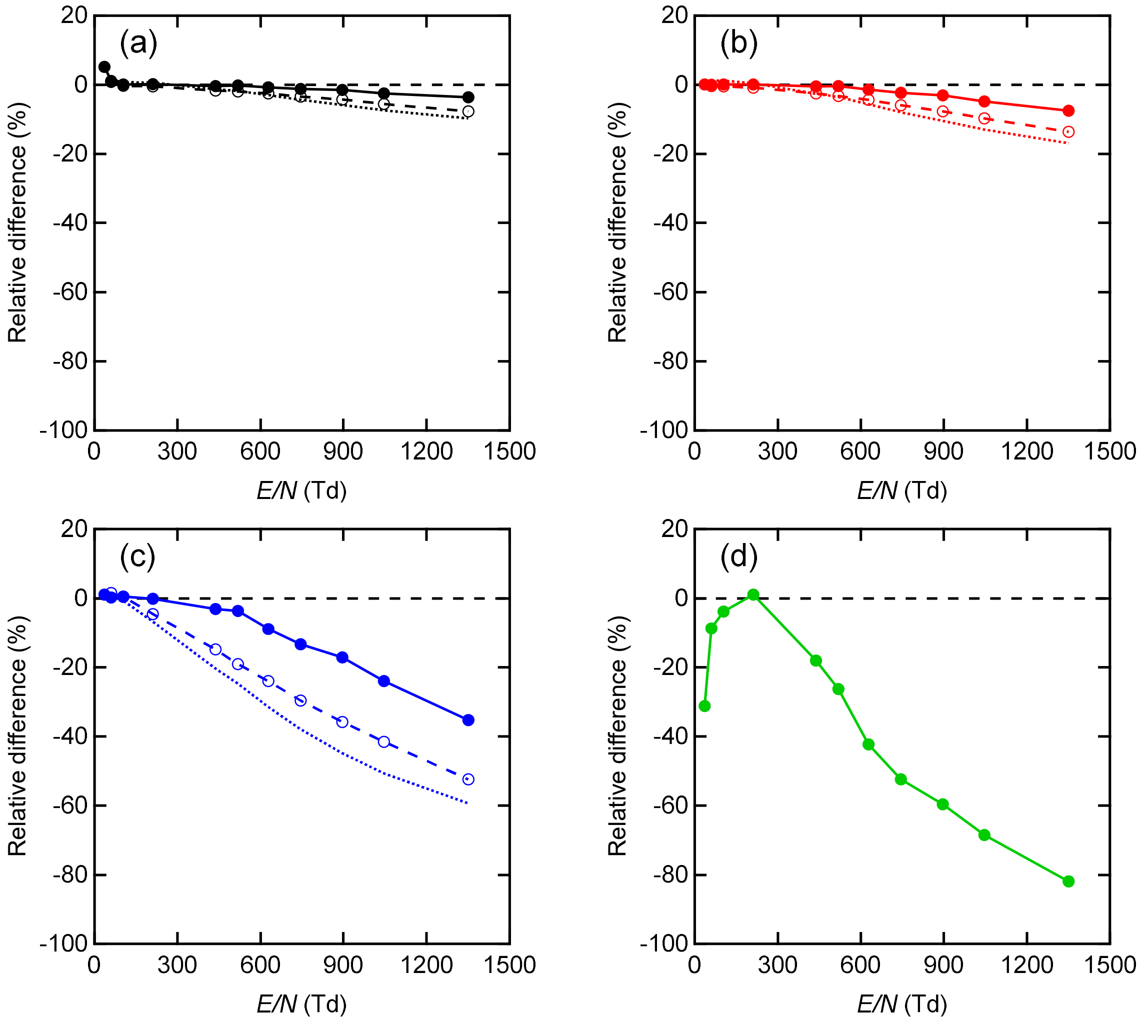

Figure 4. Relative difference for the ω parameter. (a) ω_0, (b) ω_1, (c) ω_2, and (d) ω_3. The relative differences for the ω parameter determined from discovering equations (25) and equation (34) are shown in solid lines and dashed lines, respectively. The relative differences for the ω parameter determined from fitting equation (1) to the electron swarm map are shown in dotted lines.

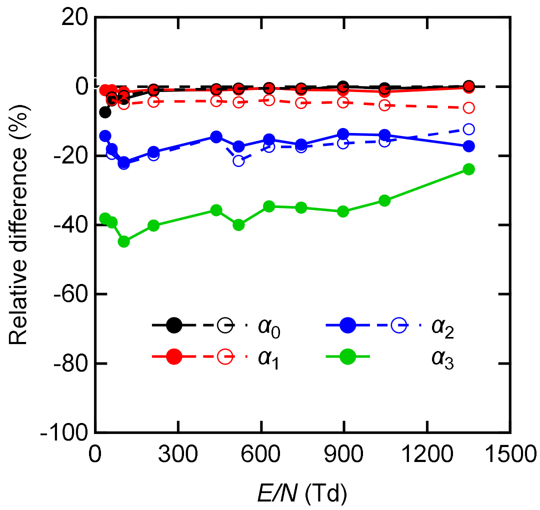

Figure 5. Relative difference for the α parameter. The relative differences for the α parameter determined from discovering equations (29) and equation (35) are shown in solid lines and dashed lines.

4.2. Electron transport coefficients in argon determined from the measured electron swarm map

Figure 6 shows the reduced ionization coefficient, α_T/N, in argon as a function of E/N. Kruithof [26], Golden and Fisher [27], Abdulla *et al*. [28], and Ishizuka *et al*. [29] measured α_T/N via the steady-state Townsend experiment. Korolov *et al*. [10] determined the value of α_T/N from their measured ionization rate coefficient, bulk drift velocity, and diffusion coefficient, according to the discussion in Ref. [30]. The value of α_T/N calculated from the MCS using the electron collision cross section sets of argon reported by Yanguas-Gil *et al*. [25] and Nakamura and Kurachi [31] is also shown. The value of α_T/N determined in this study is consistent with previously measured values and our MCS results.

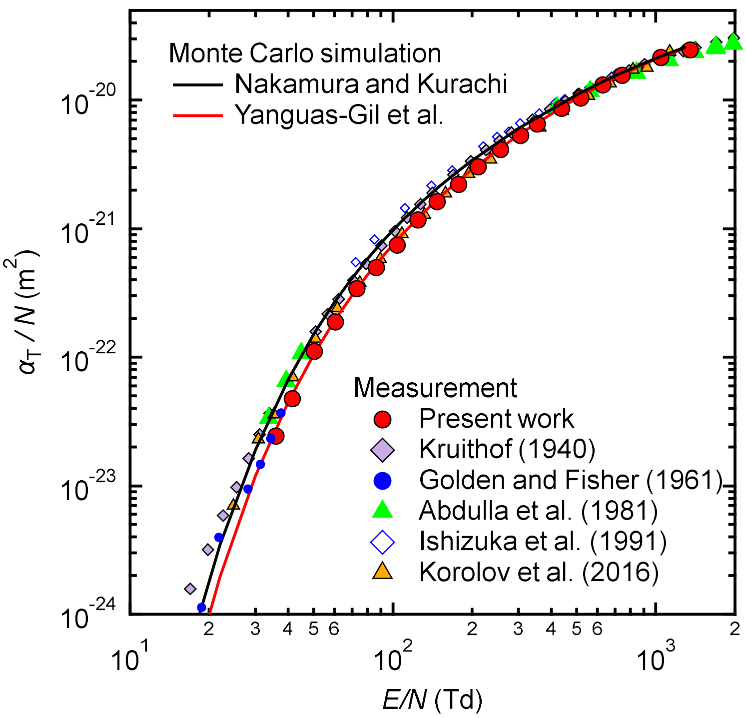

Figure 6. Reduced ionization coefficient, α_T/N, in argon. Previous data: Kruithof [26], Golden and Fisher [27], Abdulla *et al*. [28], Ishizuka *et al*. [29], and Korolov *et al*. [10]. The solid lines are our MCS results using the electron collision cross sections reported by Nakamura and Kurachi [31] and Yanguas-Gil et al. [25]

Figure 7 shows the variation in the measured and calculated ionization rate coefficients R_i/N in argon as a function of E/N. Haefliger and Franck [32] measured the value of R_i/N through the pulsed-Townsend experiment. Korolov *et al*. [10] measured the value of R_i/N by fitting equation (1) to the measured electron swarm map. The value of R_i/N determined in this study well reproduces the calculated and previously measured values of R_i/N.

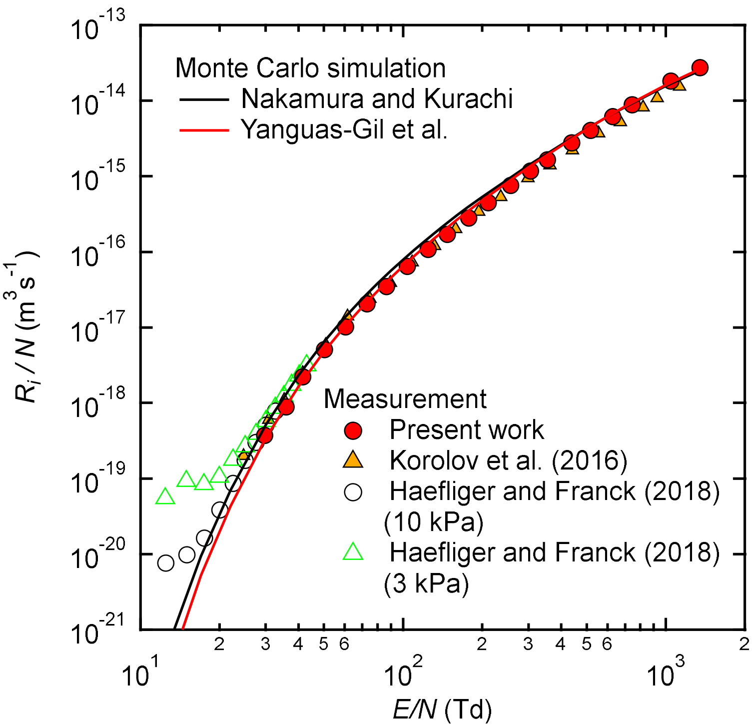

Figure 7. Ionization rate coefficient, R_i/N, in argon. Previous data: Korolov *et al*. [10]; Haefliger and Franck [32]. The solid lines are our MCS results using the electron collision cross sections reported by Nakamura and Kurachi [31] and Yanguas-Gil et al. [25]

The variation in W_r and W_m determined in this work as a function of *E/N* is shown in figure 8, together with that calculated from our MCS. The values of the electron drift velocity measured by Nakamura and Kurachi [31] and Korolov *et al.*[10] are also plotted. When ionization growth occurs, the value of the electron drift velocity depends on its definition [30]. Nakamura and Kurachi measured the electron drift velocity from the slope of the peak time of the measured arrival-time spectra (ATS) of an electron swarm against the drift distance. Their measured electron drift velocity is the peak-time drift velocity, W_p. Korolov *et al.* [10] determined the electron drift velocity from the slope of the peak position of the spatial electron distribution over time. They used equation (1) to approximate the measured electron swarm map. Under this approximation, the peak position of the spatial electron distribution is consistent with the center-of-mass of the distribution; therefore, they claimed that their determined electron drift velocity was W_r.

The values of W_r and W_m determined in this study are consistent with those calculated from our MCS. These values are almost equal and consistent with the measured value of W_p in the low *E/N* region. With increasing *E/N* values, the value of W_r becomes higher than that of W_m. The relationship between the two electron drift velocities is described as [19]

$$W_m = W_r - 2\alpha_T D_L + 3(\alpha_T)^2 Q_L - \cdots. \quad (36)$$

When the values of Q_L and high-order transport coefficients are small, equation (36) indicates $W_r > W_m$ when $\alpha_T > 0$. Such a relationship was observed in the electron swarm experiment in methane [33] as well as in the MCS in real gases [34, 35] and model gases [36].

The value of W_r determined in this study is consistent with that determined by Korolov *et al.* in the low *E/N* region; however, the two values become inconsistent with increasing *E/N* values. The previously determined value of W_r is also inconsistent with the value of W_r calculated from our MCS. The inconsistency was also remarked by Korolov *et al.*, who attributed it to the electron collision cross sections used in their calculation; however, our determined values of the electron drift velocities well reproduced the MCS results. This indicates that the peak position of the spatial electron distribution is not equal to its center of mass; therefore, the electron drift velocity determined by Korolov *et al.* is not necessarily equal to W_r.

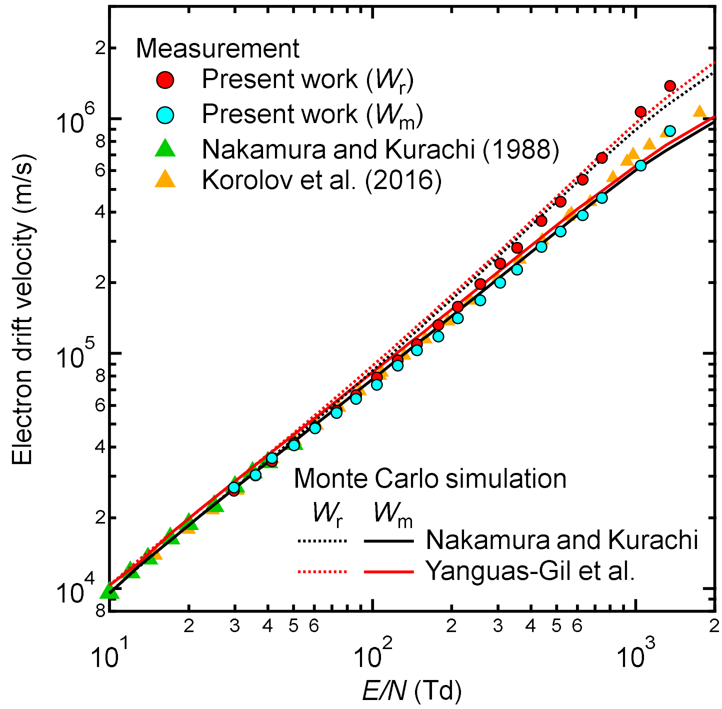

Figure 8. Electron drift velocity in argon. Previous data: Nakamura and Kurachi [31] and Korolov *et al*. [10]. The solid and dotted lines are our MCS results using the electron collision cross sections reported by Nakamura and Kurachi [31] and Yanguas-Gil et al. [25]

Figure 9 shows the value of the reduced longitudinal diffusion coefficient ND_L in argon as a function of E/N. Nakamura and Kurachi [31] determined ND_L from the characteristic width of the measured ATS. Hernández-Ávila *et al.* [37] determined ND_L from the gap currents measured in the pulsed Townsend experiment. Korolov *et al*. [10] determined ND_L by fitting equation (1) to the measured electron swarm map. The value of ND_L determined in this study is consistent with previously measured data below 300 Td and reproduces the value of ND_L calculated from our MCS.

The value of ND_L determined in this study is higher than that determined by Korolov *et al.,* which is lower than our MCS results. This discrepancy is caused by approximating the electron swarm map using equation (1). The comparison results, as shown in the electron drift velocity and longitudinal diffusion coefficient, demonstrate the necessity of considering high-order transport coefficients for the proper determination of electron transport coefficients from the electron swarm map.

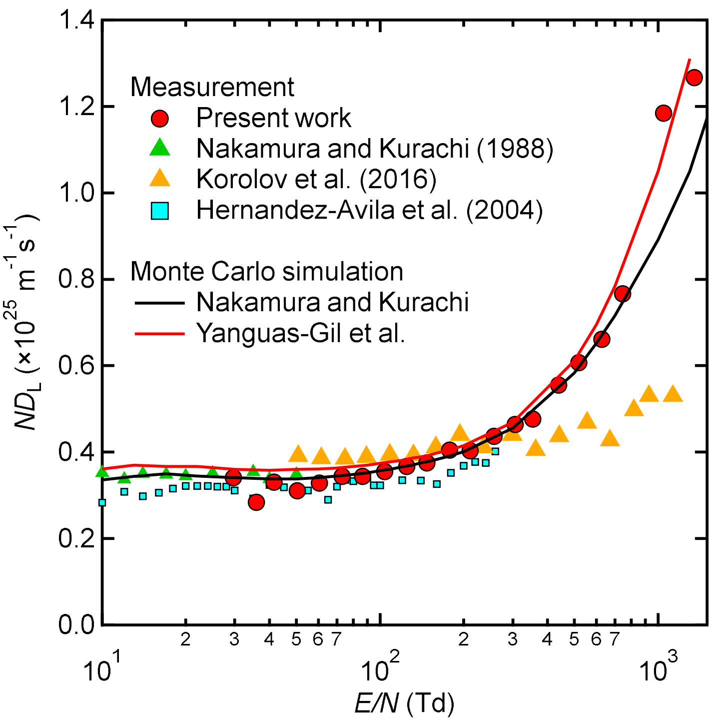

Figure 9. Reduced longitudinal diffusion coefficient, ND_L, in argon. Previous data: Nakamura and Kurachi [31]; Hernández-Ávila *et al.* [37]; Korolov *et al*. [10]. The solid lines are our MCS results using the electron collision cross sections reported by Nakamura and Kurachi [31] and Yanguas-Gil et al. [25]

The variations in $N\alpha_2$ and $N^2\alpha_3$ as functions of E/N are shown in figure 10, together with those calculated from our MCS. The values of $N\alpha_2$ and $N^2\alpha_3$ decrease monotonically with increasing E/N values. The values of $N\alpha_2$ and $N^2\alpha_3$ determined in this study are similar to those calculated from our MCS.

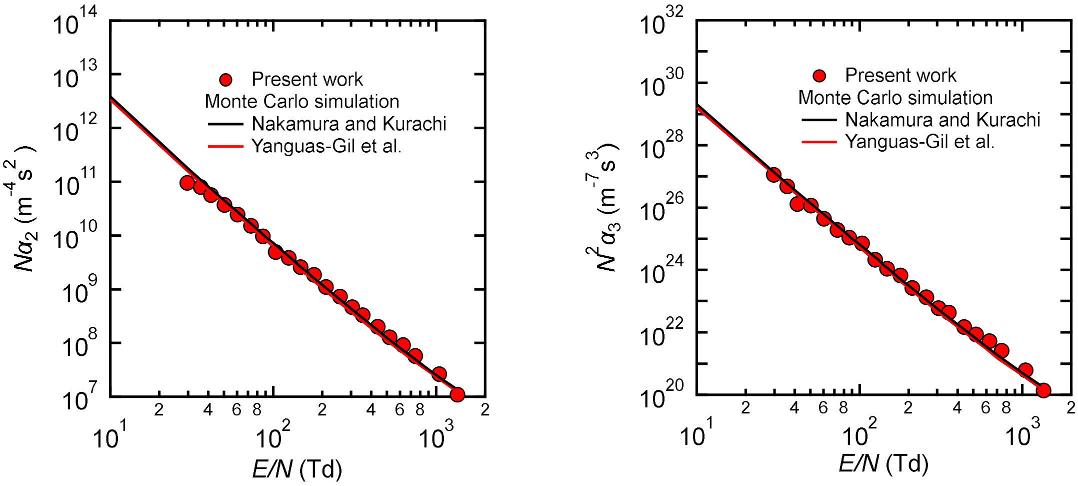

Figure 10. Variation of $N\alpha_2$ and $N^2\alpha_3$ as functions of E/N values in argon. The solid lines are our MCS results using the electron collision cross sections reported by Nakamura and Kurachi [31] and Yanguas-Gil et al. [25]

Figure 11 shows the value of the reduced longitudinal third-order transport coefficient, N^2Q_L, in argon determined from ω_3 and α parameters together with our MCS results. The value of N^2Q_L calculated from the Boltzmann equation analysis [38] is also shown. Q_L can be obtained from α parameters as [39]

$$Q_L \approx \frac{2(\alpha_2)^2}{(\alpha_1)^5} - \frac{\alpha_3}{(\alpha_1)^4}. \tag{37}$$

The physical meaning of Q_L is discussed by Simonović et al. [40]. When $Q_L \neq 0$, the electron distribution deviates from the Gaussian function. The positive value of Q_L means that the trailing edge of the electron distribution is elongated. A steep decrease of Q_L with increasing E/N values in the low E/N region is related to the Ramsauer-Townsend minimum of the elastic momentum transfer cross section of Ar [38]. The values of N^2Q_L determined from the swarm map are of the same order of magnitude as those from our MCS. The two types of N^2Q_L determined from the electron swarm map differ from each other, and the value of N^2Q_L from α parameters is close to our MCS result. As shown in figure 4, the determined values of ω_3 could have large uncertainty; therefore, the value of N^2Q_L determined from α parameters could be more reliable than that determined from ω_3.

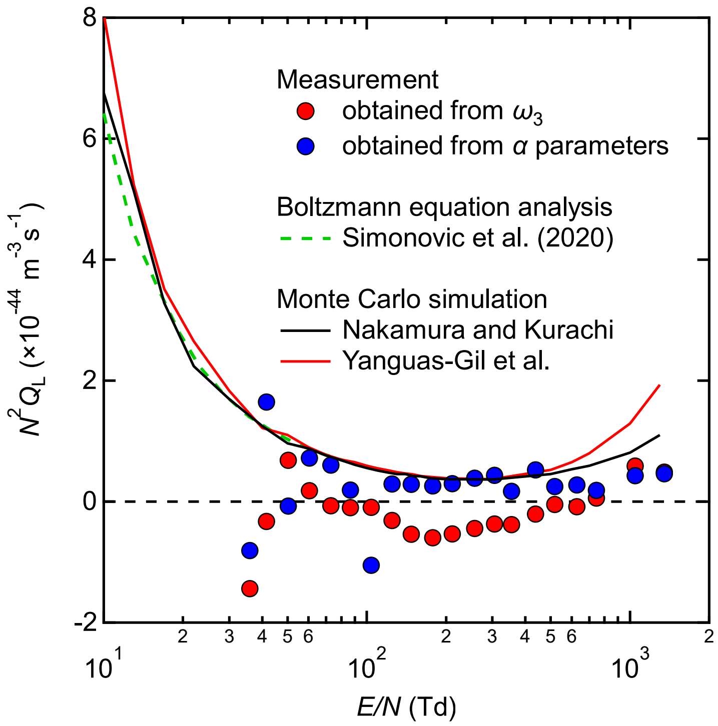

Figure 11. Reduced longitudinal third-order transport coefficient, N^2Q_L, in argon. The solid lines are our MCS results using the electron collision cross sections reported by Nakamura and Kurachi [31] and Yanguas-Gil et al. [25]

5. Conclusions

In this study, we developed a method for determining the electron transport coefficients via data-driven discovery of electron continuity equations in electron swarm maps. Our method discovers two types of electron continuity equations, allowing us to determine the ω and α parameters, which include the Townsend first ionization coefficient, α_T, ionization rate coefficient, R_i/N, , center-of-mass drift velocity, W_r, mean arrival-time drift velocity, W_m, longitudinal diffusion coefficient, D_L, and longitudinal third-order transport coefficient, Q_L. We can directly deal with the electron continuity equation using our method; therefore, assuming an analytical form of the electron swarm map is not required. This makes it easy to consider third- and higher-order transport coefficients when analyzing an electron swarm map.

In order to demonstrate the present method and clarify the importance of considering third-order transport coefficient, a benchmark study was carried out using the electron swarm map in argon calculated from the MCS. The transport coefficients determined by fitting a Gaussian function to the electron swarm map are the least consistent with the transport coefficients calculated from the MCS. We found that discovering the electron continuity equation in the electron swarm map yields more accurate transport coefficients. Considering third-order transport coefficient improves the accuracy of the transport coefficient determined using the present method. As a general trend, the transport coefficients determined using the present method becomes lower than the transport coefficients calculated from the MCS with increasing E/N values. This may indicate the need for considering higher-order transport coefficients for the proper description of the electron swarm map.

The electron transport coefficients in argon were determined using our method, from E/N = 29.7 Td to 1351.6 Td. The electron swarm map measured by a scanning drift tube experiment was used. For the α_T/N and R_i/N, the determined values were found to be consistent with the previously measurements and our MCS results. For the electron drift velocity, the determined value of W_r and W_m are consistent with the values of W_r and W_m calculated from the MCS. The determined values of W_r become larger than those of W_m with increasing E/N values, and such a tendency is consistent with the theoretical relationship between W_r and W_m. For the reduced longitudinal diffusion coefficient ND_L, the determined values are consistent with our MCS results but higher than the values of ND_L reported by Korolov et al., who determined them by curve fitting to the electron swarm map. We also determined the reduced longitudinal third-order transport coefficient, N^2Q_L, second order α parameter, $N\alpha_2$, and third-order α parameter, $N^2\alpha_3$. The transport coefficients determined in this work are valuable for assessing the electron collision cross sections of argon and plasma simulations.

Acknowledgements

The authors would like to thank M. Vass, I. Korolov, and Z. Donkó for providing numerical data on the electron swarm map measured by their scanning drift tube and kind support. This work was partly supported by JSPS KAKENHI Grant Number 22K14245.

References

[1] Petrović Z L, Dujko S, Marić D, Malović G, Nikitović Ž, Šašić O, Jovanović J, Stojanović V and Radmilović-Rađenović M 2009 Measurement and interpretation of swarm parameters and their application in plasma modelling *J. Phys. D: Appl. Phys.* **42** 194002

[2] Petrović Z L, Šuvakov M, Nikitović Ž, Dujko S, Šašić O, Jovanović J, Malović G and Stojanović V 2007 Kinetic phenomena in charged particle transport in gases, swarm parameters and cross section data *Plasma Sources Sci. Technol.* **16** S1

[3] Kawaguchi S, Takahashi K and Satoh K 2021 Electron collision cross section set for N_2 and electron transport in N_2, N_2/He, and N_2/Ar *Plasma Sources Sci. Technol.* **30** 035010

[4] Stokes P W, Foster S P, Casey M J E, Cocks D G, Gonzalez-Magana O, de Urquijo J, Garcia G, Brunger M J and White R D 2021 An improved set of electron-THFA cross sections refined through a neural network-based analysis of swarm data *J Chem. Phys.* **154** 084306

[5] Robson R, White R and Hildebrandt M 2018 *Fundamentals of Charged Particle Transport in Gases and Condensed Matter* (Boca Raton: CRC Press)

[6] Makabe T and Petrovic Z L 2015 *Plasma Electronics Applications in Microelectronic Device Fabrication* (Boca Raton: CRS Press)

[7] Kawaguchi S, Takahashi K, Satoh K and Itoh H 2016 Electron transport analysis in water vapor *Jpn. J. Appl. Phys.* **55** 07LD3

[8] Pinhão N R, Loffhagen D, Vass M, Hartmann P, Korolov I, Dujko S, Bošnjaković D and Donkó Z 2020 Electron swarm parameters in C_2H_2, C_2H_4 and C_2H_6: measurements and kinetic calculations *Plasma Sources Sci. Technol.* **29** 045009

[9] Vass M, Korolov I, Loffhagen D, Pinhão N and Donkó Z 2017 Electron transport parameters in CO_2: scanning drift tube measurements and kinetic computations *Plasma Sources Sci. Technol.* **26** 065007

[10] Korolov I, Vass M and Donkó Z 2016 Scanning drift tube measurements of electron transport parameters in different gases: argon, synthetic air, methane and deuterium *J. Phys. D: Appl. Phys.* **49** 415203

[11] Korolov I, Vass M, Bastykova N and Donko Z 2016 A scanning drift tube apparatus for spatiotemporal mapping of electron swarms *Rev. Sci. Instrum.* **87** 063102

[12] Kumar K, Skullerud H and Robson R 1980 Kinetic Theory of Charged Particle Swarms in Neutral Gases *Aust. J. Phys.* **33** 343

[13] Petrović Z L, Simonović I, Marjanović S, Bošnjaković D, Marić D, Malović G and Dujko S

2017 Non-equilibrium of charged particles in swarms and plasmas—from binary collisions to plasma effects *Plasma Phys. Control. Fusion* **59** 014026

[14] Kawaguchi S, Nakata N, Satoh K, Takahashi K and Satoh K 2021 Measurement of the third-order transport coefficient in N_2 and its effect on the longitudinal diffusion coefficient measured from the arrival-time spectra of an electron swarm *Plasma Sources Sci. Technol.* **30** 035006

[15] Rudy S H, Brunton S L, Proctor J L and Kutz J N 2017 Data-driven discovery of partial differential equations *Sci. Adv.* **3** e1602614

[16] Raissi M, Perdikaris P and Karniadakis G E 2017 Machine learning of linear differential equations using Gaussian processes *J. Compt. Phys.* **348** 683

[17] Karniadakis G E, Kevrekidis I G, Lu L, Perdikaris P, Wang S and Yang L 2021 Physics-informed machine learning *Nat. Rev. Phys.* **3** 422-40

[18] Raissi M, Perdikaris P and Karniadakis G E 2019 Physics-informed neural networks: A deep learning framework for solving forward and inverse problems involving nonlinear partial differential equations *J. Comput. Phys*. **378** 686

[19] Kondo K and Tagashira H 1990 Evolution equation and transport coefficients defined by arrival-time spectra of swarms *J. Phys. D: Appl. Phys.* **23** 1175

[20] Wang S, Teng Y and Perdikaris P 2021 Understanding and Mitigating Gradient Flow Pathologies in Physics-Informed Neural Networks *SIAM J. Sci. Comput.* **43** A3055

[21] Daw A, Bu J, Wang S, Perdikaris P and Karpatne A 2022 arXiv:2207.02338

[22] Glorot X and Bengio Y 2010 *Proceedings of the Thirteenth International Conference on Artificial Intelligence and Statistics* PMLR **9** 249-256

[23] Kingma D P and Ba J 2014 arXiv:1412.6980

[24] Skullerud H R 1968 The stochastic computer simulation of ion motion in a gas subjected to a constant electric field *J. Phys. D: Appl. Phys.* **1** 1567

[25] Yanguas-Gil Á, Cotrino J and Alves L L 2005 An update of argon inelastic cross sections for plasma discharges *J. Phys. D: Appl. Phys.* **38** 1588

[26] Kruithof A A 1940 Townsend's ionization coefficients for neon, argon, krypton and xenon *Physica* **7** 519

[27] Golden D E and Fisher L H 1961 Anomalies in Ionization Coefficients and in Uniform Field Breakdown in Argon for Low Values of *E/p Phys. Rev*. **123** 1079

[28] Abdulla R R, Dutton J and Williams A W 1981 *15th Int. Conf. on Phenomena in Ionized Gases,* p 367

[29] Ishizuka F, Shimozuma M, Kitamori K and Tagashira H 1991 Measurement of the Effective Ionization Coefficient in Ar and C_3F_8 Mixtures *IEEJ Trans. Fundam. Mater.* **111** 175

[30] Tagashira H, Sakai Y and Sakamoto S 1977 The development of electron avalanches in argon at high E/N values. II. Boltzmann equation analysis *J. Phys. D: Appl. Phys.* **10** 1051

[31] Nakamura Y and Kurachi M 1988 Electron transport parameters in argon and its momentum transfer cross section *J. Phys. D: Appl. Phys.* **21** 718

[32] Haefliger P and Franck C M 2018 Detailed precision and accuracy analysis of swarm parameters from a pulsed Townsend experiment *Rev. Sci, Instrum.* **89** 023114

[33] Hasegawa H, Date H, Yoshida K and Shimozuma M 2009 Time-of-flight observation of electron swarm in methane *J. Appl. Phys.* **105** 113308

[34] Satoh K, Ohmori Y, Sakai Y and Tagashira H 1991 Computer simulation study of correspondence between experimental and theoretical electron drift velocities in CH_4 gas *J. Phys. D: Appl. Phys.* **24** 1354

[35] Satoh K, Itoh H, Nakao Y and Takjashira H 1988 Electron swarm development in SF_6: II. Monte Carlo simulation *J. Phys. D: Appl. Phys.* **21** 931

[36] Satoh K, Hataguchi M, Itoh H, Sakai Y and Tagashira H 1994 Computer simulation study of correspondence between experimental and theoretical electron drift velocities. II. Constant total collision frequency model gases *J. Phys. D: Appl. Phys*. **27** 1480

[37] Hernández-Ávila J L, Basurto E and Urquijo J de 2004 Electron transport and ionization in CHF_3–Ar and CHF_3–N_2 gas mixtures *J. Phys. D: Appl. Phys.* **37** 3088

[38] Simonović I, Bošnjaković D, Petrović Z L, White R D and Dujko S 2020 Third-order transport coefficient tensor of electron swarms in noble gases *Eur. Phys. J. D* **74**, 63

[39] Kawaguchi S, Takahashi K and Satoh K 2018 Expression of longitudinal third-order transport coefficient in terms of α parameters and its validity *Plasma Sources Sci. Technol.* **27** 085006

[40] Simonović I, Bosnjaković D, Petrović Z L, Stokes P, White R D and Dujko S 2020 Third-order transport coefficient tensor of charged-particle swarms in electric and magnetic fields *Phys Rev E* **101**, 023203